

Medical Physics Letter

X-ray acoustic computed tomography with pulsed x-ray beam from a medical linear accelerator

Liangzhong Xiang, Bin Han, Colin Carpenter, Guillem Pratx, Yu Kuang, and Lei Xing^{a)} Department of Radiation Oncology, School of Medicine, Stanford University, Stanford, California 94305

(Received 23 October 2012; revised 19 November 2012; accepted for publication 27 November 2012; published 18 December 2012)

Purpose: The feasibility of medical imaging using a medical linear accelerator to generate acoustic waves is investigated. This modality, x-ray acoustic computed tomography (XACT), has the potential to enable deeper tissue penetration in tissue than photoacoustic tomography via laser excitation.

Methods: Short pulsed (μ s-range) 10 MV x-ray beams with dose-rate of approximately 30 Gy/min were generated from a medical linear accelerator. The acoustic signals were collected with an ultrasound transducer (500 KHz central frequency) positioned around an object. The transducer, driven by a computer-controlled step motor to scan around the object, detected the resulting acoustic signals in the imaging plane at each scanning position. A pulse preamplifier, with a bandwidth of 20 KHz-2 MHz at -3 dB, and switchable gains of 40 and 60 dB, received the signals from the transducer and delivered the amplified signals to a secondary amplifier. The secondary amplifier had bandwidth of 20 KHz-30 MHz at -3 dB, and a gain range of 10–60 dB. Signals were recorded and averaged 128 times by an oscilloscope. A sampling rate of 100 MHz was used to record 2500 data points at each view angle. One set of data incorporated 200 positions as the receiver moved 360°. The x-ray generated acoustic image was then reconstructed with the filtered back projection algorithm.

Results: The x-ray generated acoustic signals were detected from a lead rod embedded in a chicken breast tissue. The authors found that the acoustic signal was proportional to the x-ray dose deposition, with a correlation of 0.998. The two-dimensional XACT images of the lead rod embedded in chicken breast tissue were found to be in good agreement with the shape of the object.

Conclusions: The first x-ray acoustic computed tomography image is presented. The new modality may be useful for a number of applications, such as providing the location of a fiducial, or monitoring x-ray dose distribution during radiation therapy. Although much work is needed to improve the image quality of XACT and to explore its performance in other irradiation energies, the benefits of this modality, as highlighted in this work, encourage further study. © 2013 American Association of Physicists in Medicine. [http://dx.doi.org/10.1118/1.4771935]

Key words: x-ray acoustic computed tomography (XACT), linear accelerator, photoacoustic imaging, radiation therapy

I. INTRODUCTION

Laser-based photoacoustic tomography (PAT) has become a subject of intense research because of its potential for numerous applications in clinical medicine and preclinical research. ^{1–9} PAT can create multiscale multicontrast images of living biological structures ranging from organelles to organs. This emerging technology overcomes the high degree of scattering of optical photons in biological tissue by utilizing the photoacoustic effect. ^{10–12} So far, the photoacoustic response to optical radiation with visible and near-infrared wavelength has been studied. Little attention is paid to the photoacoustic mechanisms in the x-ray region as it is believed that the peak power density of conventional x-ray source is generally insufficient to induce detectable ultrasound signal. However, early studies found that ultrasound could be produced from a polychromatic synchrotron-generated x-ray

source, which had sufficient power density (7 μ J/mrad). ^{13,14} X-ray scatter in tissue is much lower than that of optical photons, thus the advantage of an x-ray irradiation source is the deeper penetration as compared to laser excitation, which would increase the number of suitable clinical applications. X-ray acoustic computer tomography (XACT) might also provide dosimetric information during radiation therapy because the acoustic amplitude is proportional to the x-ray absorption.

In this letter, we report the first theoretical and experimental study of XACT by combining x-ray excitation and ultrasound detection. Both a reconstruction technique for XACT and two-dimensional XACT images of a metal object are presented. We investigate the relationship between the acoustic signal output and the x-ray dose and possible mechanisms involved in generating acoustic signals from x-rays.

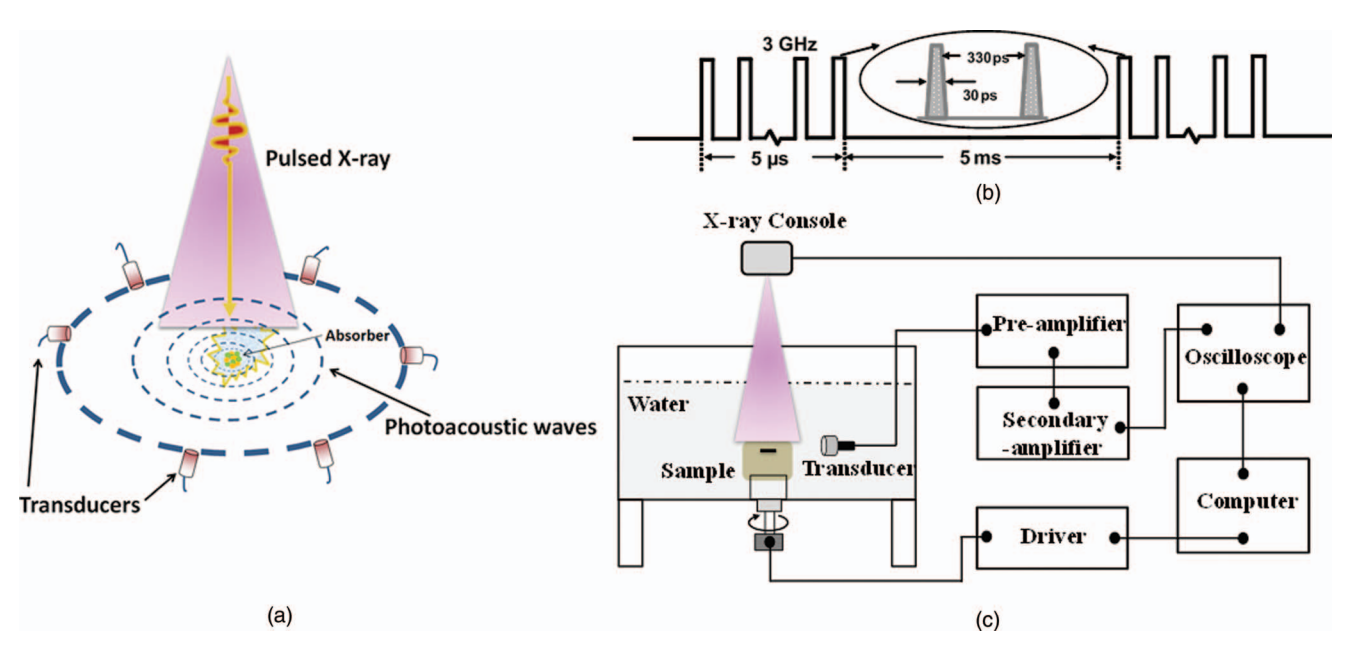


FIG. 1. Illustration of x-ray acoustic tomography. (a) Schematic of x-ray acoustic signal generation and detection. (b) Time diagram of pulsed x-ray beams from a medical linear accelerator. (c) Schematic of x-ray acoustic computer tomography system.

II. MATERIALS AND METHODS

II.A. Theory

The basic schematic of XACT is illustrated in Fig. 1(a). To induce the x-ray acoustic effect, x-rays are absorbed by the excitation of inner-shell electrons and induce photoelectrons. 15 The excited atom decays either by electromagnetic radiation, which may be reabsorbed, or by an Auger process. Auger electrons and photoelectrons transfer part of their kinetic energy to the surrounding medium by the production of cascades of secondary electrons. After many collisions these electrons are close to thermal equilibrium. The transfer of energy from the system of thermalized excited electrons to the system of atoms in the solid is governed by the electron phonon interaction, which increases the temperature of the lattice. The rise in temperature of the absorber generates the pressure waves, p, which are detected as an x-ray acoustic signal. The x-ray acoustic pressure produced by the x-ray heat source H(r, t) obeys the following equation: ¹⁶

$$\nabla^2 p(\mathbf{r}, t) - \frac{1}{v_s^2} \frac{\partial^2}{\partial t^2} p(\mathbf{r}, t) = -\frac{\beta}{C_p} \frac{\partial}{\partial t} H(\mathbf{r}, t), \tag{1}$$

where β is the isobaric volume expansion coefficient, v_s is the speed of sound, and C_p is the specific heat. For convenience, we choose the transducer position as the origin of the coordinates, so the pressure, p, at transducer position, r; and time, t, can be expressed as

$$p(\mathbf{r},t) = \left. \frac{\beta}{4\pi C_p} \iiint \frac{d\mathbf{r}}{r} \frac{\partial H(\mathbf{r},t')}{\partial t'} \right|_{t'=t-\frac{r}{c}}, \tag{2}$$

where r = |r|. H(r, t) can be expressed as H(r, t) = A(r)I(t), where A(r) is the x-ray spatial absorption distribution and I(t) is the temporal x-ray illumination function.

In practice, because of the finite bandwidth of an ultrasound transducer, recorded acoustic signals $p_d(t)$ are the convolutions of induced x-ray acoustic pressures p(t) and the impulse response h(t) of the transducer, which can be expressed as $p_d(t) = p(t)*h(t)$.

The x-ray absorption A(r) within the sample at a given position r is 17

$$\oint_{|r|=v_s t} A(\mathbf{r}) dS = \frac{4\pi C_P kt}{\beta r} \text{IFFT} \left(\frac{P_d(\omega) W(\omega)}{P_0(\omega)} \right) \frac{tk}{r_0}, \quad (3)$$

where k is a parameter depending on the absorption property of the point source and the parameters of the irradiating x-rays and $P_d(\omega)$ is the Fourier transforms of $P_d(t)$, and $W(\omega)$ is a window function used to band-limit the signals. By using a back-projection algorithm, the pressure at each time point is projected (assigned) to each point on the sphere. The integration of the object value yields the pressure, as shown in Fig. 4(b).

II.B. Imaging system

The schematic of the experimental setup is shown in Fig. 1(c). A clinical linear accelerator (Linac), (TrueBeam, Varian Medical Systems, Palo Alto, CA) was used to provide 10 MV x-ray pulses. A typical pulse sequence is 30 ps/pulse; $\sim\!15\,000$ pulses are grouped in a packet of pulses for total time of $\sim\!5~\mu s$ as shown in Fig.1(b). For radiation therapy, a typical dose to the patient is $\sim\!2$ Gy/fraction and $\sim\!30-38$ fractions in total. In our experiment, the x-ray dose-rate is approximately 30 Gy/min. The size of the x-ray beam is 50 mm \times 20 mm at the isocenter in the plane perpendicular to the beam in the experiments. The x-ray acoustic signal generated by the x-ray pulses was captured by unfocused ultrasound transducer (V301-SU, Olympus-NDT, Waltham, MA, USA) which has

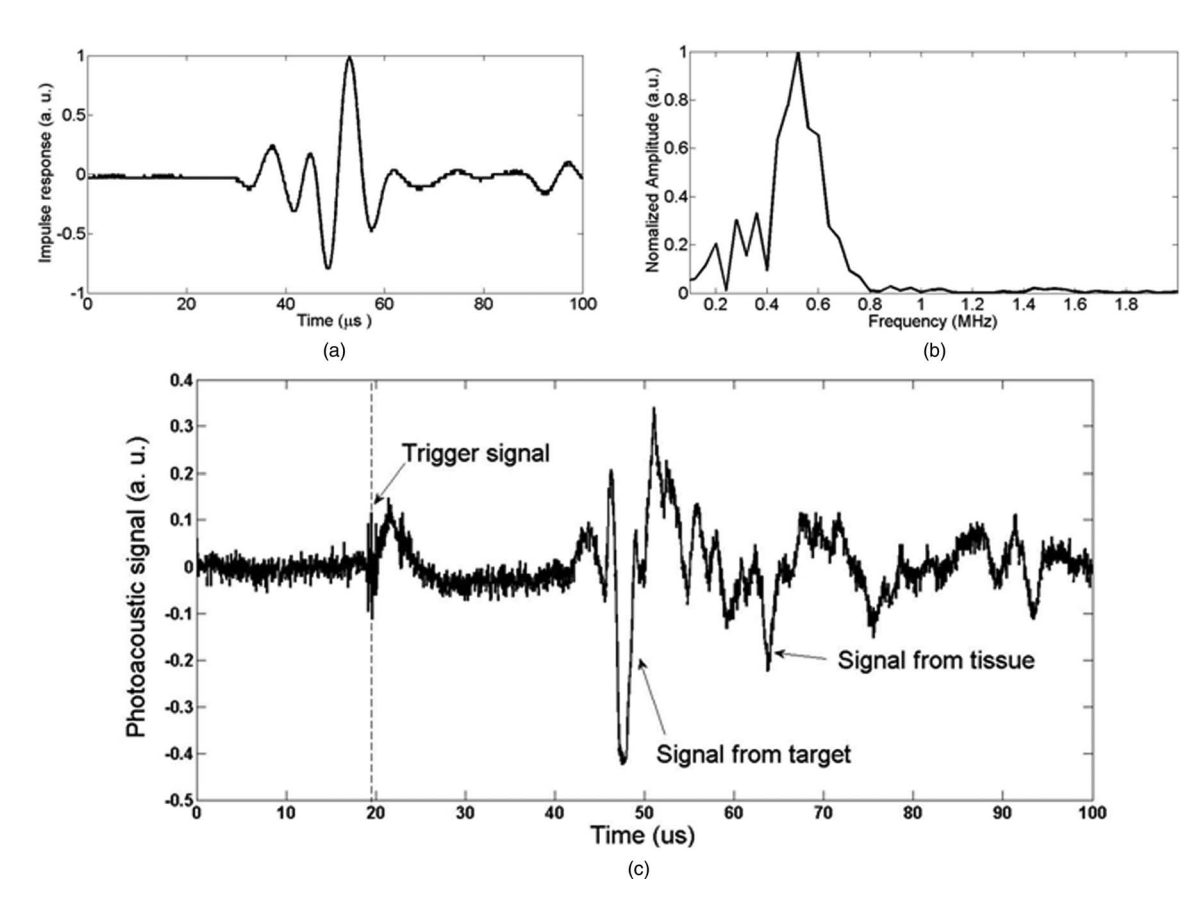


FIG. 2. X-ray acoustic signal measurement. (a) Impulse response h(t) of the transducer; (b) FFT spectrum of h(t); and (c) the x-ray acoustic signal from the object at a distance of 40.5 mm.

a central frequency of 500 kHz and a diameter of 25.4 mm. The transducer, driven by a computer-controlled step motor to scan around the sample, detected the x-ray acoustic signals in the imaging plane at each scanning position. A pulse preamplifier (5660B, Olympus-NDT, Waltham, MA, USA), which has bandwidth of 20 KHz-2 MHz at -3 dB, and switchable gains of 40 and 60 dB received the signals from the transducer and delivered the amplified signals to a secondary amplifier (PREAMP2-A, Ultratek Inc, Concord, CA, USA). The secondary amplifier has bandwidth of 20 KHz−30 MHz at −3 dB and gain range of 10-60 dB. Signals were recorded and averaged 128 times by oscilloscope (Tektronix TDS 1002C-EDU, Richarson, Texas, USA). A sampling rate of 100 MHz was used to record 2500 data points at each view angle. All control codes were written using LabVIEW graphic programming language (National Instruments, TX, USA). One set of data incorporated 200 positions as the receiver moved 360°. The XACT image was then reconstructed with the filtered back projection algorithm. 17–19

III. RESULTS

In the first experiment, we investigated x-ray acoustic signal generation with a commercial ultrasound transducer with a central frequency of 500 kHz. A lead rod with a square cross section of 4 mm \times 4 mm was irradiated to generate the x-ray acoustic signals. Figure 2(a) shows the temporal profile of the transducer impulse response h(t) of the transducer used in

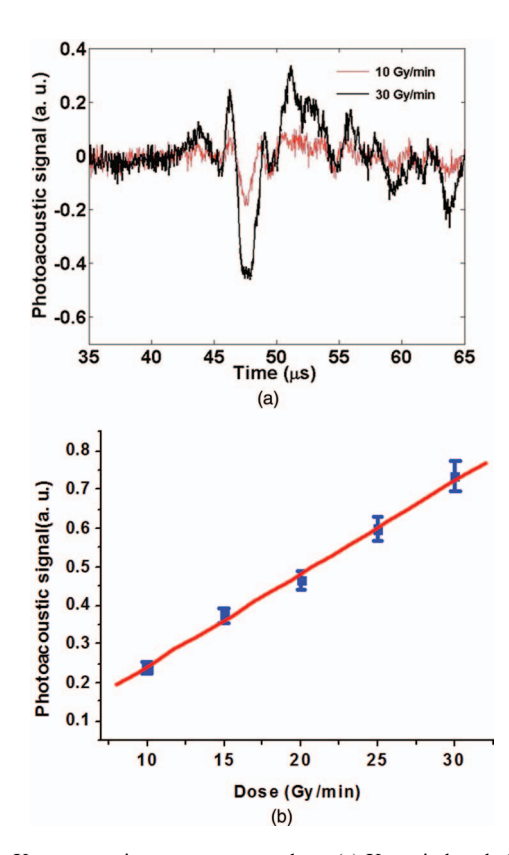


FIG. 3. X-ray acoustic output vs x-ray dose. (a) X-ray-induced ultrasound signal with different x-ray photon dose and (b) x-ray acoustic output vs dose increased.

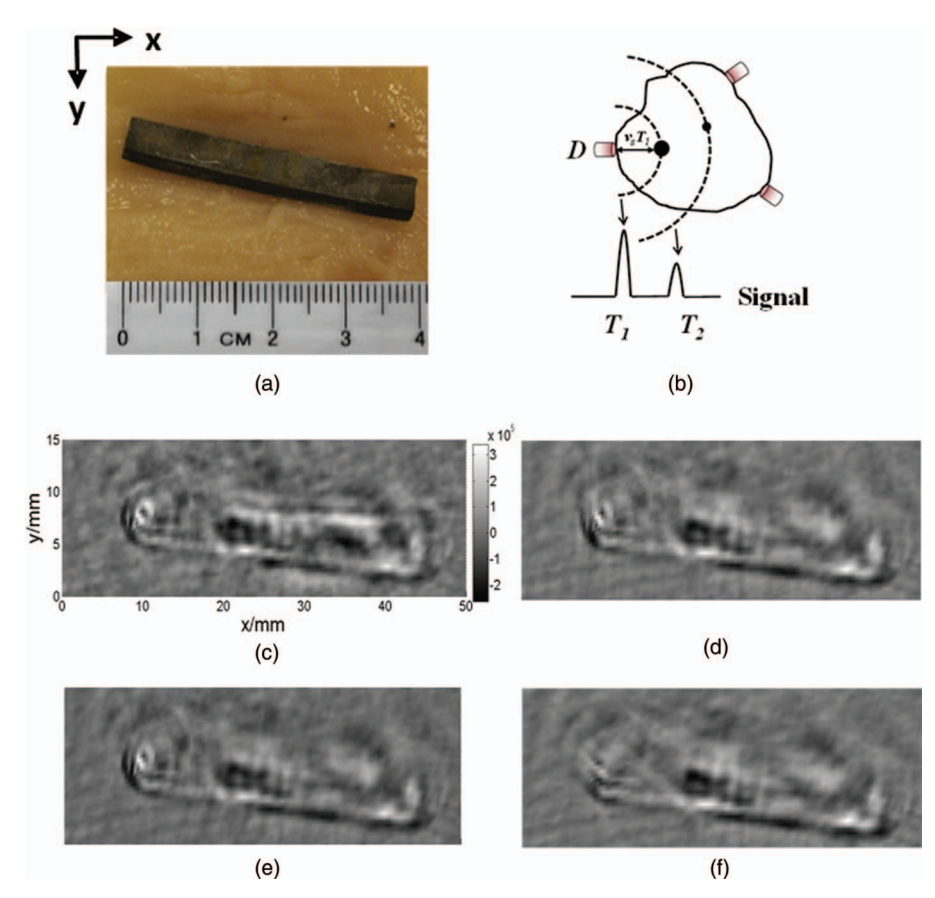


FIG. 4. Two-dimensional computer tomography of a metal object in a biological tissue. (a) Photograph of the sample composed of a piece of lead rod imbedded in chicken breast tissue. (b) Illustration of x-ray acoustic imaging reconstruction. The ultrasonic transducer at position D records the x-ray acoustic signals on a spherical surface with radius V_sT . (c) Reconstructed XACT images of the sample in 360° . (d)–(f) Images reconstructed from the data corresponding to the phantom in Fig. 4(a) with different detection angles 180° , 135° , and 90° , respectively.

this study. The fast Fourier transform (FFT) was performed on h(t) and the spectrum data h(f) is shown in Fig. 2(b). The long dimension of the rod was perpendicular to the ultrasound transducer. A major peak is readily observed in the signals [Fig. 2(c)]. The major peak width was about 2.6 μ s, which is equivalent to the acoustic time delay between the front and rear boundary of the lead rod. When we translated the lead rod, the peak moved accordingly. Thus, the acoustic signal that was measured was produced by the x-ray absorption of the metal object.

To determine the relationship between ultrasound output and x-ray dose deposition, serial x-ray acoustic signals were recorded in Fig. 3(a) with varying x-ray dose. The target was placed at the same target-transducer distance. The tube voltage of the x-ray system was set to 10 MV. The dose was linearly increased 10–30 Gy/min with a constant Linac energy. X-ray acoustic signals were acquired with the same transducer; the signal was digitized and averaged 128 times with an oscilloscope. The resulting peak-to-peak amplitude, plotted as a function of x-ray dose is given in Fig. 3(b). Figure 3(b) shows significant linearity correlation coefficient of 0.998, p < 0.001. This result indicates the x-ray acoustic signal amplitude is linear with x-ray dose deposition.

Figure 4 shows the two dimensional XACT images [Figs. 4(c)-4(f)] and the photo of a lead rod imbedded of

chicken breast tissue [Fig. 4(a)]. The center of the image is the origin of the circular scanning orbit of the transducer. The reconstructed image represents the x-ray absorption deposition distribution. Therefore we compare only the size and shape of the rod in the XACT image in Fig. 4(c) and the corresponding photo Fig. 4(a). We found that the recovered size of the rod diameter was about 3.9 mm, in good agreement with the actual object size of 4 mm. Figures 4(c)-4(f) display the reconstructed image with different limitedview scanning. When the scanning angle is relatively wide $\theta > 135^{\circ}$, the filtered back-projection method provides a relatively high contrast image. Both the position and the shape of the sources can be clearly identified from the image [Figs. 4(c)–4(e)]. However, when the scanning angle $\theta < 90^{\circ}$, the reconstructed image is blurred. This limited view reconstruction thus causes artifacts and interface blurring.²⁰ The reconstructed XACT image agrees well with the cross section of the original phantom in terms of size and relative location of the target boundary which demonstrates the potential for in vivo imaging.

IV. DISCUSSION AND CONCLUSION

We have developed the XACT technique based on the detection of acoustic signals generated by the pulsed x-ray beam

from a linear accelerator. We presented the results of our theoretical and experimental investigations on the new imaging modality. The x-ray acoustic signals from a lead rod embedded in chicken breast tissue were clearly detected by the system and the results were in good agreement with the known shape of the object, which demonstrates the feasibility of the proposed approach. The conversion from x-ray to ultrasonic energy is an interesting observation in physics and presents a new uncharted area for research and applications. Fundamentally, x-ray acoustic signal arises from the differential absorption and scattering of x-ray photons. Theoretically, 30 Gy delivered from x-ray radiation induces an estimated <10 mK temperature rise in the absorber;²¹ this temperature rise is on the same order (20 mK) as that of a photoacoustic laser pulse of energy density of $\sim 10 \text{ mJ/cm}^2$. Similar to x-ray luminescence computed tomography (XLCT),^{22,23} XACT is inherently a dual modality imaging technique capable of providing acoustic imaging information in addition to the transmission x-ray image. A selective excitation scheme as implemented in XLCT to image samples containing unknown distributions of x-ray absorbing material(s). Compared to the laser-based excitation, an important advantage is that the penetration of x-ray photons is much deeper and with little scattering. Thus XACT extends the laser-based photoacoustic imaging depth limit. XACT may also provide a means for dosmiteric measurement or even in vivo dosimetry monitoring during radiation therapy because the x-ray acoustic amplitude is proportional to the x-ray absorption. Improved instrumentation for higher resolution would use a broad bandwidth ultrasound transducer and ultrashort x-ray pulses that have the ability of generating high-peak-power. This should lead to substantial enhancement in x-ray acoustic conversion efficiency and improvement of spatial resolution. 10 Real-time mapping of therapeutic x-ray doses during radiation therapy may be on the horizon.²¹

ACKNOWLEDGMENTS

The work was partially supported by grants from National Institutes of Health (NIH) (1R01 CA133474 and 1R21 CA153587). The authors would like to thank Fred van den Haak for technical assistance.

- tion for contrast-enhanced imaging," Nat. Commun. **3**(618), 1–10 (2012).
- ³B. Wang *et al.*, "Photoacoustic tomography system for noninvasive real-time three-dimensional imaging of epilepsy," Biomed. Opt. Express 3, 1427–1432 (2012).
- ⁴D. Razansky, A. Buehler, and V. Ntziachristos, "Volumetric real-time multispectral optoacoustic tomography of biomarkers," Nat. Protoc. **6**, 1121–1129 (2011).
- ⁵J. Laufer *et al.*, "In vivo preclinical photoacoustic imaging of tumor vasculature development and therapy," J. Biomed. Opt. **17**, 05601601–0560160108 (2012).
- ⁶M. F. Kircher *et al.*, "A brain tumor molecular imaging strategy using a new triple-modality MRI-photoacoustic-Raman nanoparticle," Nat. Med. **18**, 829–835 (2012).
- ⁷J. W. Kim, E. I. Galanzha, E. V. Shashkov, H. M. Moon, and V. P. Zharov, "Golden carbon nanotubes as multimodal photoacoustic and photothermal high-contrast molecular agents," Nat. Nanotechnol. 4, 688–694 (2009).
- ⁸Y. G. Zeng, D. Xing, Y. Wang, B. Z. Yin, and Q. Chen, "Photoacoustic and ultrasonic coimage with a linear transducer array," Opt. Lett. **29**, 1760–1762 (2004).
- ⁹G. D. Gao, S. H. Yang, and D. Xing, "Viscoelasticity imaging of biological tissues with phase-resolved photoacoustic measurement," Opt. Lett. **36**, 3341–3343 (2011).
- ¹⁰L. H. V. Wang and S. Hu, "Photoacoustic tomography: In vivo imaging from organelles to organs," Science 335, 1458–1462 (2012).
- ¹¹S. H. Yang, F. Ye, and D. Xing, "Intracellular label-free gold nanorods imaging with photoacoustic microscopy," Opt. Express 20, 10370–10375 (2012).
- ¹²Z. J. Chen, S. H. Yang, and D. Xing, "In vivo detection of hemoglobin oxygen saturation and carboxyhemoglobin saturation with multiwavelength photoacoustic microscopy," Opt. Lett. 37, 3414–3416 (2012).
- ¹³W. Sachse and K. Y. Kim, "Observation of x-ray generated ultrasound," IEEE Trans. Sonics Ultrason. 32, 677–680 (1985).
- ¹⁴M. E. Garcia, G. M. Pastor, and K. H. Bennemann, "Theory for the photoacoustic response to x-ray absorption," Phys. Rev. Lett. 61, 121–124 (1988).
- ¹⁵Y. Fang, A. N. Vasilev, and V. V. Mikhailin, "Theory of x-ray photoacoustic-spectroscopy," Appl. Phys. A: Mater. Sci. Process. 60, 333–341 (1995).
- ¹⁶R. A. Kruger, P. Y. Liu, Y. R. Fang, and C. R. Appledorn, "Photoacoustic ultrasound (Paus) Reconstruction tomography," Med. Phys. 22, 1605–1609 (1995).
- ¹⁷Y. Wang, D. Xing, Y. G. Zeng, and Q. Chen, "Photoacoustic imaging with deconvolution algorithm," Phys. Med. Biol. 49, 3117–3124 (2004).
- ¹⁸L. Z. Xiang *et al.*, "Real-time optoacoustic monitoring of vascular damage during photodynamic therapy treatment of tumor," J. Biomed. Opt. **12**, 01400101–01400108 (2007).
- ¹⁹G. Hu and B. He, "Magnetoacoustic imaging of electrical conductivity of biological tissues at a spatial resolution better than 2 mm," PLoS ONE 6, e2342101–e2342109 (2011).
- ²⁰Y. Xu, L. V. Wang, G. Ambartsoumian, and P. Kuchment, "Reconstructions in limited-view thermoacoustic tomography," Med. Phys. 31, 724–733 (2004).
- ²¹J. Medin, C. K. Ross, G. Stucki, N. V. Klassen, and J. P. Seuntjens, "Commissioning of an NRC-type sealed water calorimeter at METAS using Co-60 gamma-rays," Phys. Med. Biol. 49, 4073–4086 (2004).
- ²²G. Pratx, C. M. Carpenter, C. Sun, R. P. Rao, and L. Xing, "Tomographic molecular imaging of x-ray-excitable nanoparticles," Opt. Lett. 35, 3345–3347 (2010).
- ²³C. M. Carpenter, C. Sun, G. Pratx, R. Rao, and L. Xing, "Hybrid x-ray/optical luminescence imaging: Characterization of experimental conditions," Med. Phys. 37, 4011–4018 (2010).

a) Electronic mail: lei@stanford.edu

¹L. Z. Xiang *et al.*, "Photoacoustic molecular imaging with antibody-functionalized single-walled carbon nanotubes for early diagnosis of tumor," J. Biomed. Opt. **14**, 02100801–02100807 (2009).

²K. Wilson, K. Homan, and S. Emelianov, "Biomedical photoacoustics beyond thermal expansion using triggered nanodroplet vaporiza-